Journal of Crystal Growth 416 (2015) 47–56

Contents lists available at ScienceDirect

Journal of Crystal Growth

journal homepage: www.elsevier.com/locate/jcrysgro

The crystal morphology and growth rates of triclinic N-docosane crystallising from N-dodecane solutions

Diana M. Camacho [a], Kevin J. Roberts [a,*], Ken Lewtas [b], Iain More [b]

[a] Institute of Particle Science and Engineering and Institute of Process Research and Development, School of Chemical and Process Engineering, University of Leeds, Leeds LS2 9JT, UK
[b] Infineum UK Ltd, Milton Hill Business and Technology Centre, Abingdom OX13 6BB, UK

ARTICLE INFO

Article history:
Received 27 October 2014
Received in revised form
6 January 2015
Accepted 9 January 2015
Communicated by S.R. Qiu
Available online 16 January 2015

Keywords:
A1. Morphological analysis
A1. BFDH and zone axis methods
A1. Crystal growth kinetics and rates
A1. In-situ optical microscopy
A1. Kinetic roughening
B1. N-alkanes

ABSTRACT

A detailed analysis of the crystal morphology of triclinic n-docosane ($C_{22}H_{46}$) is presented together with a preliminary assessment of the supersaturation-dependence of the growth rates for the predicted (*hkl*) faces. A methodology to index the experimentally observed crystal faces, based on a combined BFDH and zone axis methodology is defined. Analysis using this methodology yields the morphological indexation of n-docosane to be (001), (112), (102), (010), and (1 − 33) or (130) based on the expected triclinic crystal structure. Crystals of n-docosane growing from supersaturated n-dodecane ($C_{12}H_{26}$) solutions, as studied using in-situ optical microscopy, at three different supersaturation (σ) levels 0.01, 0.02 and 0.05, reveal that the crystal morphology changes with increasing in supersaturation, evolving from a habit consistent with a triclinic crystal system to a habit that is perhaps more representative of an orthorhombic structure. Growth rates determined for the (112) and (102) faces as well as for those less dominant faces range between 0.51 and 9.85 μm/s, in good agreement with previously reported data for other organic molecules including n-alkanes.

© 2015 The Authors. Published by Elsevier B.V. This is an open access article under the CC BY-NC-ND license (http://creativecommons.org/licenses/by-nc-nd/4.0/).

1. Introduction

The crystallisation behaviour of n-alkanes (C_nH_{2n+2}) has been the subject of numerous studies due to its importance in practical applications, especially in terms of understanding their role with respect to the cold flow behaviour of fuels. Previous work using single crystal and powder X-ray diffraction have characterised the solid-state properties for some of these compounds, suggesting they follow an overall scheme, in terms of the expected crystal structures as a function of the parity (n) of the number of carbon atoms within the molecule to be as follows: – triclinic, for n-alkanes with even carbon number $6 \leq n \leq 26$; – monoclinic, for $26 \leq n \leq 36$; and – orthorhombic for $n \geq 36$, and also for n odd $11 \leq n \leq 39$ [1].

In this respect, n-docosane crystallises in a triclinic structure, $Z=1$, $P\bar{1}$, with unit cell parameters $a=4.289$, $b=4.823$, $c=29.544$, $\alpha=86.237$, $\beta=70.661$ and $\gamma=72.097$ [2] in good agreement with the predictions of Nyburg and Potworowski [3].

Most single long-chain n-alkanes with carbon chain lengths >26, generally grow from solutions as rhombic-shaped thin platelets with large and well-developed (001) faces together with much smaller (110) side faces. Polygonized growth spirals [4,5] have been observed on the (001) faces when grown from n-alkane solutions (hexane and heptane) [6]. This is consistent with n-alkane solvent molecules incorporating as impurities. Growth from more complex solvents (cyclohexane) was found to result in no observable growth defects (spirals) [7]. Although, these particular crystals are typically bounded by (110) faces some additional small faces can occur for orthorhombic and for monoclinic phases for growth near equilibrium and this often results in a crystal morphology with a more “hexagonal” habit [7].

Although the bulk crystallisation of n-alkanes has been studied extensively [2,8–14], the dynamics of this process and the complex nature of their crystal morphology have not so far allowed an extensive investigation to be made into their growth kinetics. Single long-chain n-alkane solutions systems crystallise comparatively easily and are characterised by small metastable zone widths (MSZW). This is associated with very fast lateral growth in which fully faceted crystals can be difficult to observe. Additionally, both the small thickness of the crystals together with the

Abbreviations: Cif, Crystallographic information file; BCF, Burton–Cabrera–Frank model; BFDH, Bravais–Friedel–Donnay–Harker model; B&S, Birth and Spread model; RIG, Rough Interface Growth model; 2D, Two dimensional; 3D, Three dimensional

* Correspondence to: Institutes of Process R&D (iPRD) & Particle Science & Engineering (IPSE), School of Chemical and Process Engineering (SCaPE) Room 2.20, Engineering Building, University of Leeds, Leeds LS2 9JT, UK. Tel.: +44 113 343 2408, 2404; fax: +44 113 343 2384.
E-mail address: k.j.roberts@leeds.ac.uk (K.J. Roberts).

http://dx.doi.org/10.1016/j.jcrysgro.2015.01.006
0022-0248/© 2015 The Authors. Published by Elsevier B.V. This is an open access article under the CC BY-NC-ND license (http://creativecommons.org/licenses/by-nc-nd/4.0/).

List of symbols

d_{hkl}	Inter-planar distances within morphological (*hkl*) forms
MSZW	Metastable zone width
R	Single face growth rate ($\mu m\ s^{-1}$)
T	Solution temperature (K)
T_d	Equilibrium dissolution temperature (K)
T_c	Crystallisation temperature (K)
x	Mole fraction of solute in solution
σ	Relative supersaturation
ΔH_d	Molal enthalpy of dissolution $\left(J\ mol^{-1}\right)$
ΔS_d	Molal entropy of dissolution $\left(J\ mol^{-1}\ K^{-1}\right)$

– very low birefringence in the direction normal to the dominant morphological form add to the difficulty of their observation using polarised light microscopy.

In spite of this, some studies have been carried out to measure the growth rates of individual faces. For instance, in the case of n-octacosane ($C_{28}H_{38}$) and n-hexatriacontane ($C_{36}H_{74}$), the observed crystals displayed a thin-lozenge plate-like morphology with well-developed (001) faces together with smaller (110) faces. Analysis of the growth rate kinetics measurements of the (110) faces was consistent with a dislocations-mediated [15] or two dimensional nucleation [16] growth mechanism for n-octacosane and n-hexatriacontane crystals, respectively. The observed crystal growth rates for these systems were found to be below 14 μm/s for supersaturations σ in the range of 0.007–0.15. The dominant (001) faces in the case of n-hexatriacontane crystals was found to develop by the slow incorporation of growth units by surface diffusion at the surface steps defined by the growth spirals [17,18].

In the case of the lower chain length n-alkane crystals, whose morphology is determined by crystallisation into the triclinic structure, such studies are scarcer due, in part, to the greater complexity in terms of preparing single crystals, controlling their growth and determining their corresponding crystal morphology. Some observations on the morphology of n-tetracosane ($C_{24}H_{50}$) crystallising from both n-hexane and n-octane solutions have been presented in Liu X-Y and Bennema P [19], together with the prediction of their morphologies using different models. However, the determination of the face-specific growth kinetics of these crystals has not as of yet been reported. Previous studies have been limited to only the development of instrumentation for collection of experimental data, e.g. associated with attempts to study the kinetics of n-eicosane ($C_{20}H_{42}$) crystallising from n-dodecane solutions [20].

This paper builds on this previous body of work and addresses both the assessment of the crystal morphology and the measurement of the growth rates of the individual faces, for the lower chain length n-alkane crystals. For this purpose n-docosane crystals growing from n-dodecane were studied as a function of solution supersaturation.

2. Materials and methods

2.1. Materials

Both n-docosane $C_{22}H_{46}$, the solute, and n-dodecane $C_{12}H_{26}$, the solvent, were purchased from Sigma-Aldrich. The purity of both materials was higher than 99% and no further purification was carried out.

2.2. Experimental apparatus for crystal growth measurements

In-situ crystal growth studies were carried out using an experimental set-up described earlier [21]. This comprised an inverted optical polarising microscope (Olympus Optical IMT-2), operated in bright field transmission mode, which was integrated with a Lumenera Infinity 3.3 megapixel CCD camera which captured crystal images as a function of time. The images were then analysed using the INFINITY ANALYSE software (http://www.lumenera.com/support/downloads/microscopy-downloads.php). The associated growth cell comprised a simple temperature-controlled annular tank (diameter 11 cm, depth 3.5 cm) sealed with two removable circular glass plates. The solution was secured within a 0.5 ml sealed UV glass cuvette with a path length of 1 mm which was placed within the cell as close to the objective lens of the microscope as feasible. The temperature within the cell was measured using a PT100 temperature probe and controlled using a Haake F3 circulating water bath that circulates water through the growth cell. The overall system is shown in Fig. 1.

2.3. Experimental procedure

The solubility and MSZW for n-docosane in n-dodecane solutions was measured using turbidimetric methods [22]. The solubility was modelled according to the van't Hoff equation:

$$\ln x = -\frac{\Delta H_d}{RT} + \frac{\Delta S_d}{R} \quad (1)$$

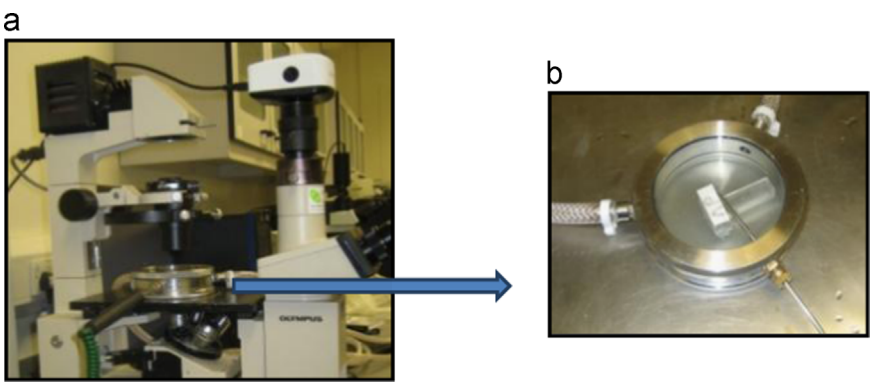

Fig. 1. Experimental set up for crystal growth rates measurements, after [21]. (a) Olympus IMT-2 inverted optical polarising microscope integrated with Lumenera Infinity 3.3 megapixel CCD camera. (b) Enlarged picture of the crystal growth cell.

where x is the mole fraction of the solute in the solution, T(K) is the solution temperature, $\Delta H_d (J/\text{mol})$ is the molal enthalpy of dissolution, $\Delta S_d (J/\text{mol K})$ is the molal entropy of dissolution and R $(8.314 (J/\text{mol K}))$ is the gas constant.

The fitted parameters obtained were $\Delta H_d = 63135.9 \pm 617.6$ J/mol and $\Delta S_d = 198.84 \pm 2.19$ (J/mol K).

The examination of the crystal growth rates was carried out by crystallising n-docosane from a supersaturated n-dodecane solution at a concentration of 350 g/l, for which the measured MSZW was found to be 1.9 °C corresponding to equilibrium dissolution T_d and crystallisation T_c temperatures of 24.7 and 22.8 °C, respectively.

The supersaturation required for crystallisation was created by decreasing the solution's temperature from T_d to three different temperatures within the metastable zone; 24.6, 24.5 and 24.1 °C corresponding to supersaturations σ of 0.01, 0.02 and 0.05 respectively. Although the supersaturation was set by decreasing the solution's temperature by circulating water through the cell, the growth of the crystals was only measured after the targeted temperature had been established as shown in Fig. 2. The supersaturation level at each temperature is calculated using expression (2)

$$\sigma = \frac{x}{x_e} - 1 \tag{2}$$

where x_e is the molar fraction of the solute in the solution at equilibrium, obtained from the van't Hoff equation at the temperature of measurement.

The crystal morphology and subsequent growth of the observed crystals were followed by recording images at equal time-intervals, every 30 s for the two lowest σ and every 20 s for the highest σ. The growth rates of the individual faces (R) were obtained by following the increase with time of the normal distance from the centre of the projected two dimensional ($2D$) crystal to the faces as shown in Fig. 3. This is a good approximation of the advancement of the corresponding ($hk0$) faces as the growth rate of the expected dominant (001) face can be of around two orders of magnitude lower. As the micrographs were collected using the microscope in brightfield mode, the contrast of the image edges was found to be very low in terms of their reproduction here. Therefore, as an aid to presentation, a perimeter to the crystals was drawn by visual examination using the tools in the image analysis software, in order to delimit the morphology of the crystals and facilitate the subsequent analysis of their respective growth rates. The crystals' centre was further defined drawing lines that connected the crystals' corners defined by the two most important observed faces.

For the most dominant faces ten to thirteen measurements of the normal distance increase were obtained, while for occasional faces appearing with the crystal growth two to seven measurements were recorded.

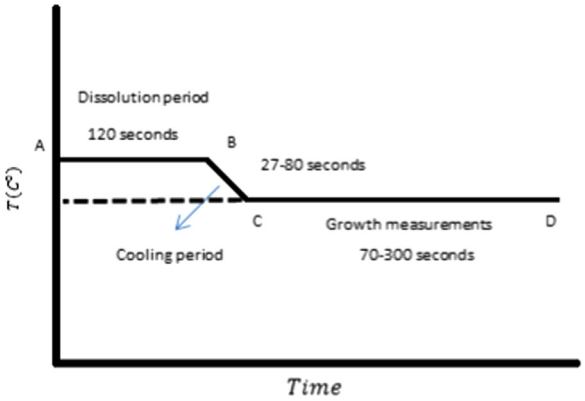

Fig. 2. Description of the methodology used to reach the temperature at which the growth rate are measured. Typical values of the temperature profile for each segment are: AB (120 s), BC (27–80 s), CD (70–300 s).

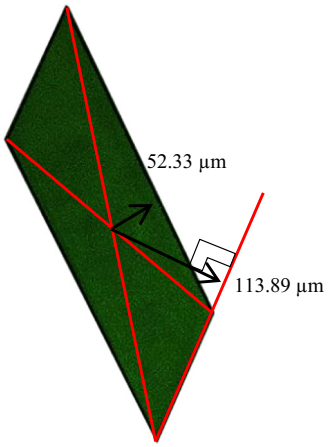

Fig. 3. Example of measurement of normal distances from the centre of the projected (2D) crystal to the faces. The distances were obtained using the INFINITY ANALYSE software by drawing a perpendicular line to each face from the centre of the crystal.

2.4. Crystal growth mechanism

The crystal growth mechanism was investigated by fitting $R(\sigma)$ dependence to models representing different interfacial crystal growth mechanisms, in particular:

- The Burton–Cabrera–Frank (BCF) model [23] which follows a parabolic tendency with growth being mediated by presence of screw dislocations on the crystal surface:

$$R = A\sigma^2 \tanh\left(\frac{B}{\sigma}\right) \tag{3}$$

- The birth and spread (B&S) model [24] which follows an exponential tendency with growth mediated by two-dimensional ($2D$) nucleation:

$$R = A\sigma^{5/6} \exp\left(\frac{B}{\sigma}\right) \tag{4}$$

- The rough interface (RIG) model [25] which follows a linear tendency as the growth occurs on a molecularly roughened surface:

$$R = A\sigma \tag{5}$$

where A and B are system-related constants.

2.5. Morphological analysis

The assessment of the n-docosane crystal morphologies was carried out using modelling routines available in both Material Studio (http://accelrys.com/products/materials-studio/) and Mercury 3.1. (http://www.ccdc.cam.ac.uk/Solutions/CSDSystem/Pages/Mercury.aspx). The former was used to initially obtain an estimation of the likely crystal morphology by applying the Bravais [26], Friedel [27], Donnay and Harker [28] (BFDH) model, including a consideration of all possible Miller indices for comparison with the observed morphologies. This approach relates the external shape of a crystal to the internal crystallographic lattice dimensions and symmetry and states that:

"After allowing for the reduction of the growth slide thickness from space group symmetry considerations, the most morphologically

important forms (*hkl*), and hence those with the lowest growth rates, are those having the greatest inter-planar distance d_{hkl}".

Using the known triclinic unit cell parameters for n-docosane, a crystallographic information file (cif) was produced which provided a list of the most likely crystallographic planes, with the likelihood of their occurrence determined by the in ranking with respect to the highest d_{hkl} spacings. Using the BFDH approach, d_{hkl} spacings can be taken as being inversely proportional to the perpendicular distance from the centre of the crystals to the corresponding face, which in turn can be considered as a measure of the relative growth rate for the simulation of the crystal morphology.

The list of Miller indices obtained was subsequently re-arranged by grouping the lattice planes with respect to those having a common zone axis [*uvw*], – defined – as a crystallographic axis perpendicular to the set of two dimensional (2D) planes (*hkl*) satisfying the relationship

$$uh+vk+wl=0 \tag{6}$$

The indices of the zone axis [*uvw*] are defined with respect to two of its constituent lattices planes $(h_1k_1l_1)$, $(h_2k_2l_2)$ by:

$$\frac{u}{\begin{bmatrix} k_1 & l_1 \\ k_2 & l_2 \end{bmatrix}} = \frac{v}{\begin{bmatrix} l_1 & h_1 \\ l_2 & h_2 \end{bmatrix}} = \frac{w}{\begin{bmatrix} h_1 & k_1 \\ h_2 & k_2 \end{bmatrix}} \tag{7}$$

The planes with the lowest order of their Miller indices within each group were then examined in pairs, by modifying the corresponding cif. file in Mercury 3.1., to iteratively obtain morphology predictions onto the basal (001) plane, i.e. the most representative plane of the observed plate-like crystals. These projections were segmentally compared with the micrographs of the crystals obtained experimentally. Essentially the law of rational indices was used, to define possible indices for the pairs of faces whose mutual orientation was consistent with the predictions. The results obtained were then combined and ranked in terms of the coincidental indices present in each pair, in order to generate putative crystal morphologies that satisfied the various pair-wise simulations.

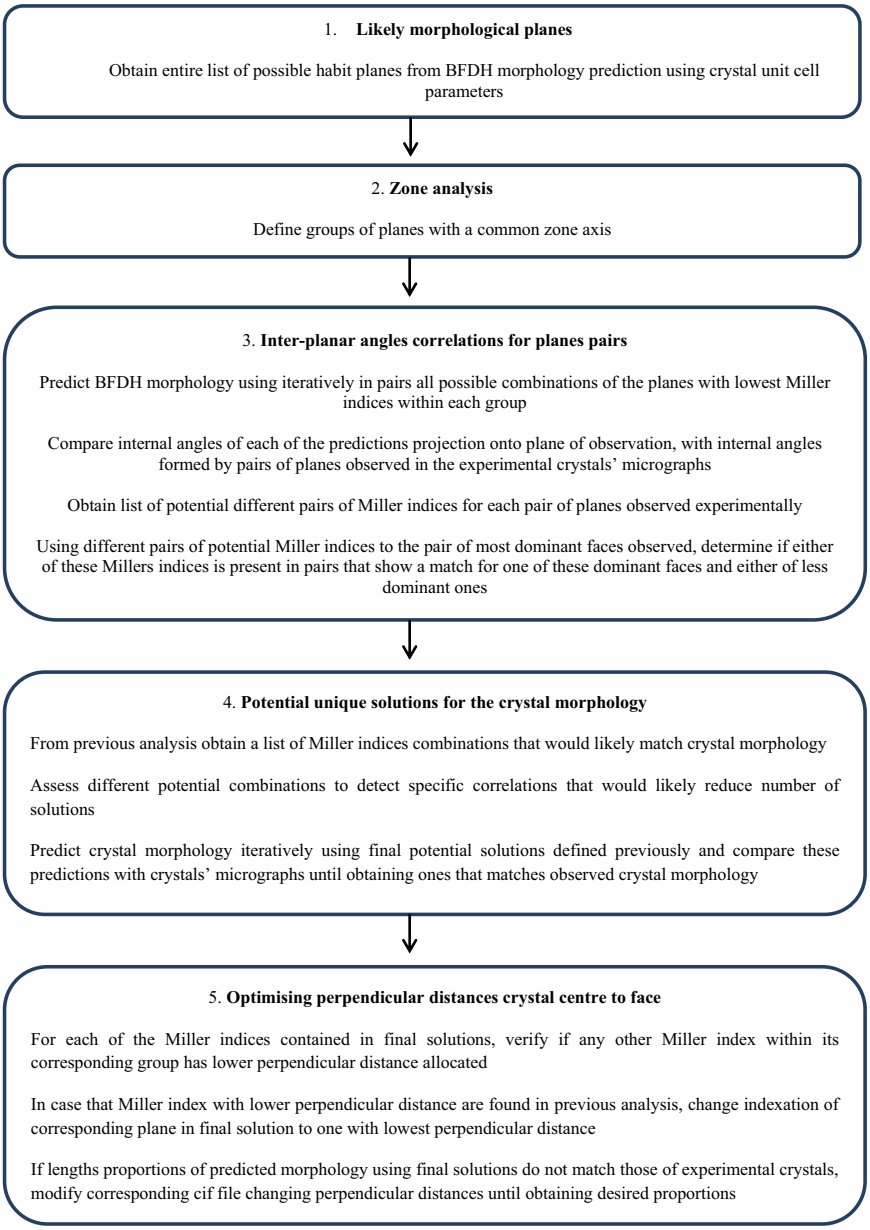

Fig. 4. Flow chart describing the procedure to follow for the morphology indexation of observed n-docosane crystals, using iterative predictions of the BFDH morphology.

Finally, once acceptable matches between the predicted and observed crystal edge orientations had been identified, the respective lengths of the projected edges in the predicted morphologies were adjusted in order to match their respective proportions as observed in the experimental observations. The latter was facilitated by varying the centre to face normal distances provided in the corresponding cif file. A schematic diagram summarising this overall methodology is given in Fig. 4.

3. Results and discussion

3.1. Crystal growth and morphological observations

Due to the very small MSZW of the system studied, i.e. ca. 2 °C, which is typical for n-alkanes systems [8,9,29,30], the growth and development of individual n-docosane crystals could only be followed within this limited temperature region resulting in only three different solution supersaturations being practical for this study. Although the value of the highest relative supersaturation σ at which the observations were done only reached 5%, kinetic roughening of the side faces was already found to manifest itself at this point, thus further limiting the range for kinetic measurements even more. Additionally, the difficulty of growing faceted crystals only allowed single measurements to be obtained for the crystal growth at each supersaturation value and even within this limited range of measurements a significant amount of time (ca. a month) was required to carry out the experimental work.

Due to the very thin plate-like crystals observed, also typical of n-alkanes, the quality of the microscopy images obtained using brightfield illumination did not allow easy reproduction of the data obtained. Nonetheless, these observations were found to be sufficient to assess both the crystal morphology and growth rates for the individual habit faces. A representative sequence of these micrographs for the growth of the crystals observed at each supersaturation is shown in Fig. 5.

An assessment of these morphologies reveals that the crystal habit of the n-docosane crystals changed with increasing

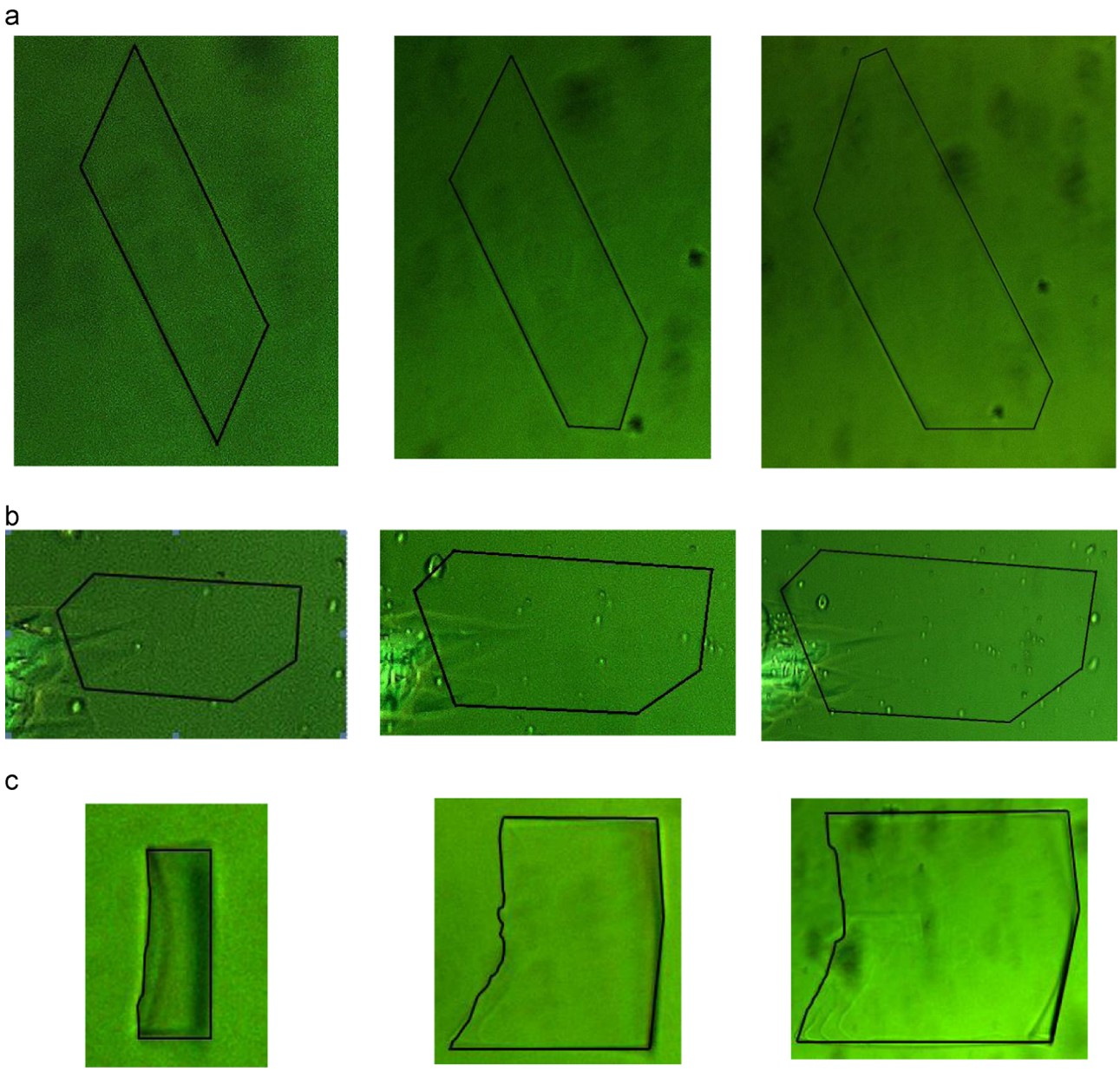

Fig. 5. Optical micrographs showing the evolution of the growth of n-docosane crystals growing from a supersaturated n-dodecane solution for three different solution supersaturations (σ). The micrograph shown are a representative sequence of the crystal growth process at (a) 24.6 °C (σ=0.01); (b) 24.5 °C (σ=0.02); (c) 24.1 °C (σ=0.05).

supersaturation from an irregular polygon towards a more regular – shape. The regular quadrilateral shape of the crystals at higher supersaturation could suggest a new molecular arrangement in the crystal structure changing from the triclinic form expected to an orthorhombic structure more typical of even parity n-alkanes growth in the presence of a homologous impurity [8,9]. The latter might be consistent with solvent incorporating at the higher supersaturations. In n-alkane crystallisation, is well known that the incorporation of lower carbon chain length n-alkanes into the lattices of crystals of even higher carbon chain lengths, can influence the arrangement of the molecules into the crystal structure. However, even if this was the case the morphology observed at the highest supersaturation is not genuinely in agreement with that expected from a crystal structure based on an orthorhombic crystal system, where a lozenge shaped morphology dominated by four symmetrically equivalent {110} faces has been previously observed [16,31].

Although the micrographs obtained at the two lowest supersaturations seemed to be associated with different crystal's morphology a close comparisons of them revealed three coincidental internal angles that would allow the same indexation for three of the crystal faces. A fourth face in each case, however, was not found to be equivalent and would thus need independent indexation. In the case of the crystals obtained at the highest supersaturation, the indexation of the faces was not carried out as its morphology was not consistent with that associated with the same triclinic crystal structure.

3.2. Morphological indexing

The prediction for the morphology observed at the two lowest supersaturations was carried out following the procedure presented in Fig. 4. Mindful of the anisotropy of the known unit cell parameters for n-docosane with the magnitude of c > > a, b the indexation for the large crystal face was taken to be {001}. BFDH analysis revealed 104 predicted crystal habit planes, including the dominant (001) plane, and 103 other possible indexations for the other four planes observed in the experimental morphology. In this case many of the d_{hkl} spacings were found to be very close and therefore, according to the methodology, these results were arranged by grouping the lattice planes into thirteen zones. These, together with the corresponding zone axis indexation, including the complete set of planes delivered by the BFDH prediction is given in the Supplementary material (SM) to this paper. Table 1. shows a summary of this information including the different calculated zone axis and some representative planes featuring the range of d spacing values observed within each group.

The inter-planar angle correlation for the planes pairs using the annotation shown in Fig. 6, revealed a set of matches for the pairs of Miller indices as presented in Table 2.

Even though in this case only one solution is possible for BC pairs, to facilitate the visualisation of the solution for the entire morphology, a general cross-checking of the pairs was carried out. This, because in each pair combination, each Miller index can be allocated to either of the faces represented by that pair. Thus, starting with the AB pairs in Table 2. and cross-checking these with the other pairs' combinations yielded the likely Miller indices for the four crystal faces observed in the micrographs as shown in Table 3.

Looking at the results in Table 3, for instance, if (230) and (010) are the most likely Miller indices for faces A and B, then the C face could take one of either three Miller indices (1 – 31), (110) or (100). Likewise the D face could take one of either four Miller indices (1 – 10), (2 – 10), (210) or (320). However, in this case as observed in Table 2, only one combination is possible for BC pairs (100) (010) and two combinations are possible for CD pairs (010) (1 – 10) or (010) (1, – 3,1). Therefore, only those set of planes in the possible solutions containing the (010) (100) and either (1–10) or (1, – 3,1) indices, would be likely to deliver the prediction for the entire crystal indexation. This is the case of the set of planes in rows one, nine and twelve of Table 3.

Arrangements of these indices considering all possible combinations among them are presented in Table 4. The comparison of the micrographs obtained at the lowest supersaturation, with the prediction of the corresponding BFDH morphology using these indices, showed that only the set of planes presented in rows one and thirteen in Table 4. would deliver a full match to the entire experimental morphology. Using these indices, further modification of the perpendicular distances from the centre of the crystal to the faces, in the corresponding cif files, gave a morphology

Table 1
List of the predicted zone axis defining the different zone groups, representative (hkl) planes and d_{hkl} spacing within each group.

Group	Zone axis [uvw]	Representative plane (hkl)	Inter-planar distance d_{hkl}
1	[100]	(010)	4.59
		(021)	2.28
		(031)	1.52
2	[010]	(100)	3.86
		(201)	1.97
		(301)	1.30
3	[1 – 10]	(110)	3.52
		(221)	1.79
4	[2 – 10]	(120)	2.30
5	[3 – 10]	(130)	1.60
6	[110]	(1 – 10)	2.59
		(2 – 21)	1.31
7	[210]	(1 – 20)	1.75
8	[310]	(1 – 31)	1.30
9	[1 – 20]	(210)	2.01
10	[3 – 20]	(230)	1.43
11	[120]	(2 – 10)	1.61
12	[1 – 30]	(310)	1.35
13	[2 – 30]	(320)	1.30

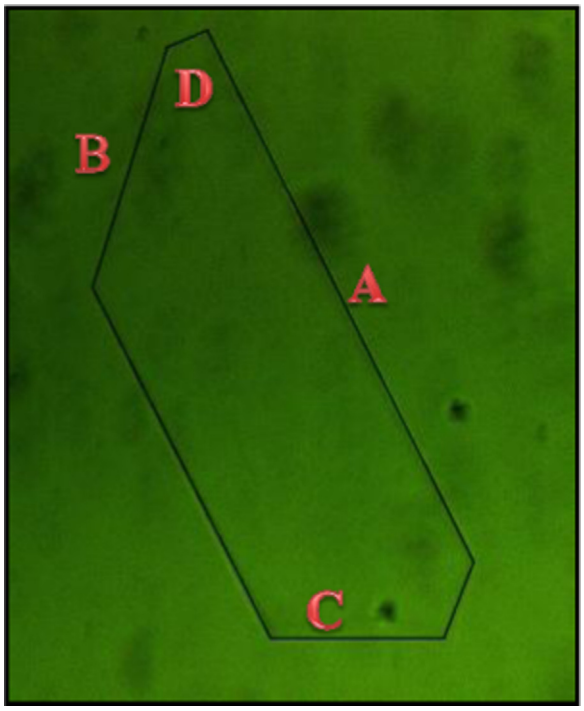

Fig. 6. Example of initial designation of crystal's faces for the morphology as observed for the lowest supersaturation (σ=0.01).

Table 2
Representative pairs of planes matching the inter-planar angles of pairs of faces for the morphology observed at the lowest supersaturation σ=0.01. Planes designated according to Fig. 6.

AB	BC	CD	AC	AD	BD
(010) (230)	(100) (010)	(1 – 10) (010)	(010) (110)	(010) (210)	(120) (320)
(010) (2 – 10)		(1 – 31) (010)	(1 – 20) (310)	(010) (320)	(100) (1 – 10)
(1 – 20) (100)			(1 – 10) (320)	(1 – 20) (110)	(100) (1 – 31)
(1 – 20) (130)			(130) (210)	(1 – 20) (320)	(1 – 10) (210)
(120) (1 – 31)			(1 – 31) (230)	(120) (2 – 10)	
(120) (210)				(100) (130)	
(100) (110)				(110) (1 – 10)	
(1 – 10) (310)				(110) (1 – 31)	
(130) (320)				(1 – 10) (230)	
(230) (310)				(1 – 31) (210)	
(2 – 10) (210)				(1 – 31) (320)	
(2 – 10) (320)				(230) (2 – 10)	

Table 3
Likely combinations of Miller indices for the four faces of the experimental crystals observed at the lowest supersaturation σ=0.01. Planes designated according to Fig. 6.

	A	B	C			D			
1	(230)	(010)	(1 – 31)	(110)	(100)	(1 – 10)	(2 – 10)	(210)	(320)
2	(230)	(310)	(1 – 31)	(1 – 20)		(1 – 10)	(2 – 10)		
3	(1 – 10)	(310)	(320)	(1 – 20)		(100)	(110)	(210)	
4	(2 – 10)	(010)	(110)	(100)		(120)	(210)	(320)	
5	(2 – 10)	(210)	(130)			(120)	(1 – 10)	(1 – 31)	
6	(2 – 10)	(320)	(1 – 10)			(120)	(1 – 20)	(1 – 31)	(120)
7	(120)	(210)	(130)			(1 – 10)	(1 – 31)		
8	(120)	(1 – 31)				(100)	(110)		
9	(1 – 20)	(100)	(010)			(110)	(1 – 10)	(130)	(1 – 31)
10	(1 – 20)	(130)	(210)			(110)	(100)		
11	(320)	(130)	(1 – 10)	(210)		(1 – 20)	(1 – 31)	(120)	(100)
12	(110)	(100)	(010)			(1 – 10)	(130)	(1 – 31)	(1 – 20)

Table 4
Potential unique solutions of the n-docosane crystals morphology observed at the lowest supersatuarion σ=0.01. Rows one and thirteen highlighted in the Table, represent the final unique solutions that match the entire crystal morphology. Planes designated according to Fig. 6.

1	(230)A	(100)C	(010)B	(1 – 10)D
2	(2 – 10)	(100)	(010)	(1 – 10)
3	(210)	(100)	(010)	(1 – 10)
4	(320)	(100)	(010)	(1 – 10)
5	(230)	(100)	(010)	(1 – 31)
6	(2 – 10)	(100)	(010)	(1 – 31)
7	(210)	(100)	(010)	(1 – 31)
8	(320)	(100)	(010)	(1 – 31)
9	(1 – 20)	(100)	(010)	(1 – 10)
10	(110)	(100)	(010)	(1 – 10)
11	(130)	(100)	(010)	(1 – 10)
12	(1 – 20)	(100)	(010)	(1 – 31)
13	(110)A	(100)B	(010)C	(1 – 31)D
14	(130)	(100)	(010)	(1 – 31)

prediction with lengths proportional to those observed experimentally.

As the planes used to carry out the analysis of the morphology were selected to represent a group of different planes with a common zone axis, then a ranking based on their respective *d*-spacing within these groups was done by using the BFDH method. (See SM).

The analysis indicated the combination (230), (010), (100), (1 – 10) to be more likely than (233), (010), (102), (1 – 13). Likewise the combination (110), (100), (010), (1 – 31) was found to be more likely than (112), (102), (010), (1 – 33). However, the later prediction is more likely to occur due to its lower indexation. As the *d*-spacing of many of the planes within each group were so close in magnitude a more detailed analysis would be required to validate these findings. It should be noted that the calculation of the attachment energy (E_{att}) could be used for this purpose; but this information requires the optimised (3*D*) crystal structure of n-docosane which is not currently available. Fig. 7. compares the most likely morphology prediction with a micrograph taken from one of the experimental crystals as observed at the σ=0.01. Likewise it presents the indexation for the morphology observed at the second supersaturation studied σ=0.02, for which the same methodology was applied. The final prediction delivers the Miller indices (112), (102), (010) for the most dominant faces and (1 – 33) and (130) for the un-coincidental less dominant faces at σ=0.01 and σ=0.02 respectively.

3.3. Crystal growth rates as a function of supersaturation

The growth rates for the individual faces of n-docosane crystals as measured at each supersaturation are presented in Fig. 8.

The growth rates for the (112) and (010) faces were found to increase as a function of supersaturation increase by 1%, while the growth of the (102) face decreases giving more importance to this face in the observed crystal morphology at σ=0.02. The higher growth rates observed at the two lower supersaturation are for the less dominant non-coincidental (1 – 33) and (130) faces. However the growth rate of the (130) face observed at σ=0.02 was found to be closer to the order of those rates observed for the (112) and (010) faces, which has an influence on the crystal morphology displayed, with the three faces having similar importance.

At the highest supersaturation σ=0.05 the morphology observed was found to have changed considerably being defined by only two faces where growth rates are significantly higher than those measured for the crystal faces at lower supersaturation. Due to the high rates of these faces, the crystal morphology displayed curvatures especially along the vertical faces (see label V in Fig. 8.), which could be consistent with the early stages of kinetic roughening. Similar findings have been reported for other organic

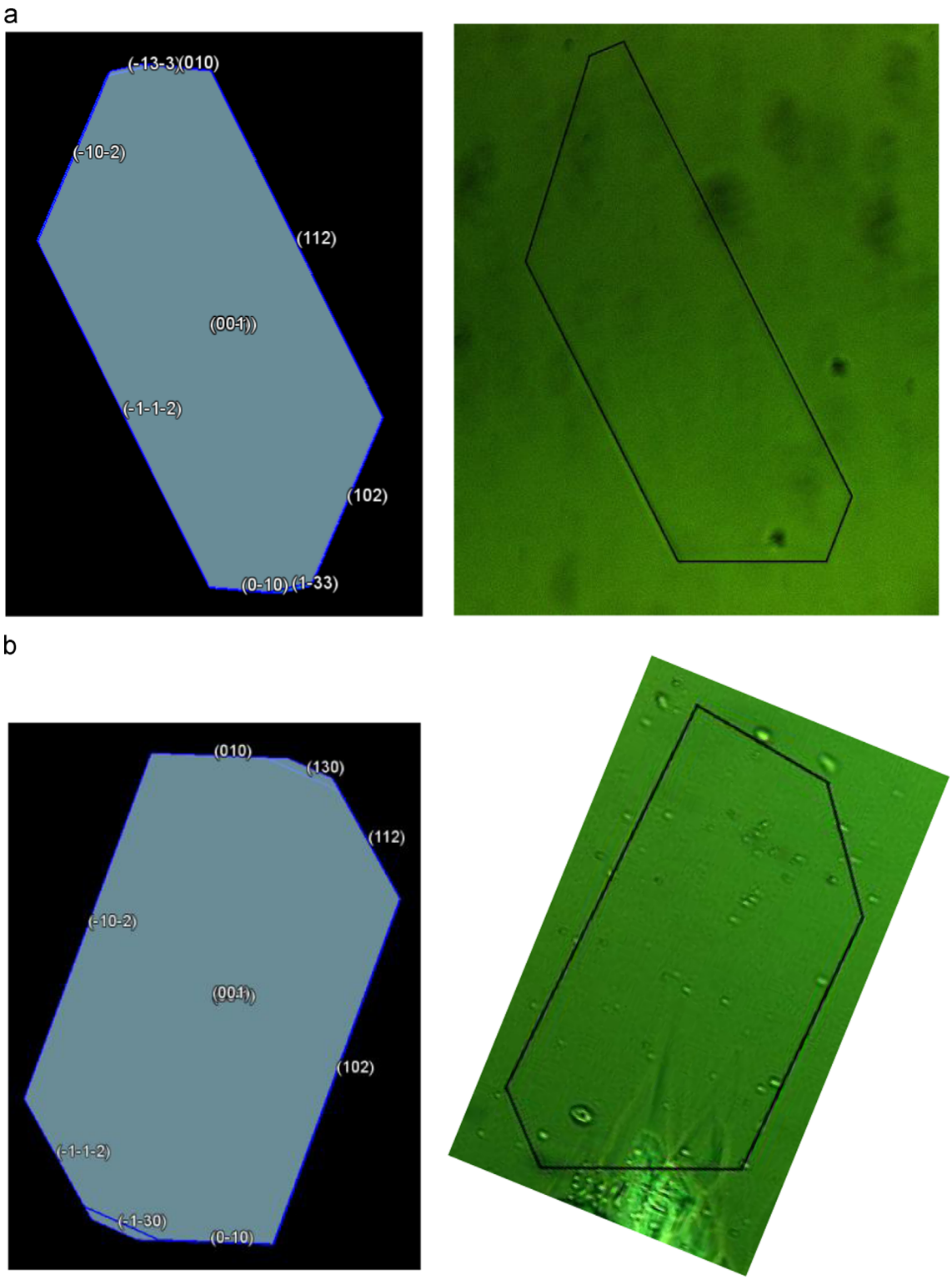

Fig. 7. Predicted BFDH morphology of n-docosane crystals using the Miller indices in the obtained unique solutions and comparison with the crystals' micrograph at two different supersaturation (a) $\sigma=0.01$ or $T=24.6$ °C and (b) $\sigma=0.02$ or $T=24.5$ °C.

materials such as biphenyl and naphthalene crystallising from toluene in which the roughening transition was observed at relative supersaturations between 1.2 and 1.5% [32]. Likewise, in the case of n-eicosane ($C_{21}H_{44}$) crystallising from n-hexane, observations of the growth morphology revealed roughening transitions to occur at relative supersaturations of around 3% [33].

A comparison of the growth rates values obtained with previously published data is shown in Table 5. These values which include those measured for similar organic systems are within the same order of magnitude of those presented in the present work.

Although the amount of experimental data collected is not sufficient at this stage to accurately assess the mechanistic regime

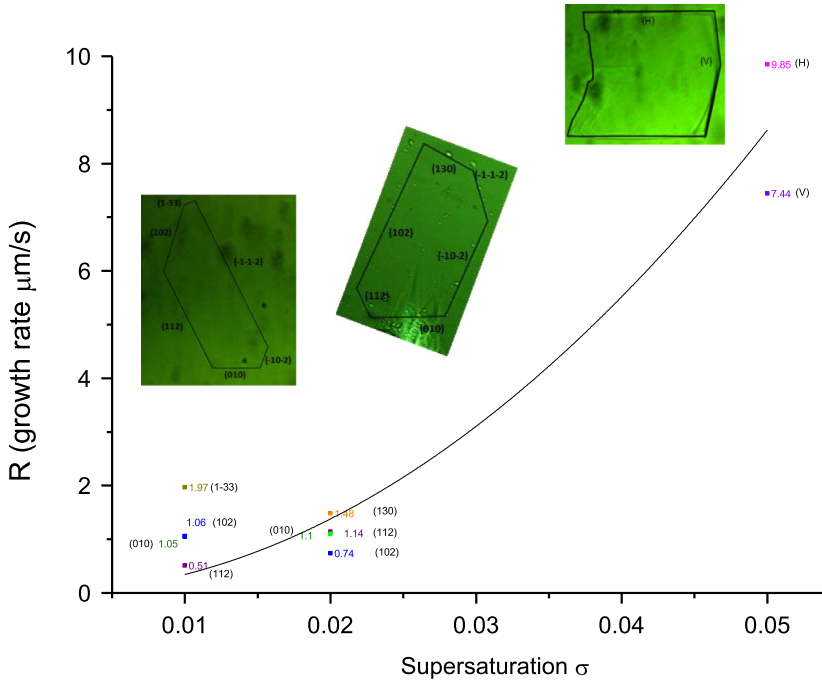

Fig. 8. Comparative growth rates of individual faces of n-docosane crystals growing from n-dodecane at three different solution's supersaturations σ=0.01, 0.02 and 0.05. Each of the colours assigned both to the symbol and *R* values represent each of the different crystal faces observed. The line represents the best fit of the data points through the BCF model.

Table 5
Comparative values of published growth rates values for individual faces of crystals of some inorganic and organic systems.

Compounds	*T* (°C)	σ	Range of growth rates (μm/s)	References
Potash alum (111)		32	0.01–0.18	[34]
L-Glutamic acid				
Length of needle-like crystals		0.47–0.5	0.025–0–0.032	[35]
Width of needle-like crystals		0.47–0.5	0.005–0–0.006	
Tripalmitin (melt)	47–52–52		0.20–0–0.45	[36]
Paracetamol in 60% methanol and 40% water		0.25	0.30	[37]
Paracetamol in the [110], [010] and [001] direction		0.06–0.26	0.020–0–0.160	[38]
Ibuprofen (001) and (011) faces in ethanol/water, ethyl acetate, acetonitrile and toluene		0.55–1.3	0.035–2.02	[21]
Hexatriacontane $C_{36}H_{74}$ in petroleum ether (110) face	17–22	0.22–0.7	0–2	[16]
Octacosane $C_{28}H_{58}$ in petroleum ether (110) face	12–22.75	0.007–0.15	0–14	[15]
Dotriacontane $C_{32}H_{66}$ in m-xylene	14.5	1–1.5	1–3	[39]
B and C polymorphs of stearic acid in butanone (110) face	16–25	0.012–0.3	0–2.8	[40]
B polymorph of stearic acid in decane (110) face		0.012–0.4	0–0.4	[41]
n-docosane in n-dodecane (010) (112) (102) and other not indexed faces	24.1–24.6	0.01–0.05	0.51–9.85	This work

of crystal growth based on $R(\sigma)$ models, a tentative assessment can still to be done. From Fig. 8. it is clear that the data points do not follow a linear relationship whilst attempts to fit the data using the B & S model does not achieve convergence. However, the data seem to follow a parabolic rate dependence and fit well to the BCF type model which would be in agreement with growth via screw dislocations. In addition to this, the growth could be limited by volume diffusion as the experiments were carried out in stagnant solutions. However, the models used here to assess the growth mechanism only consider the interaction of molecules at the crystal surface. For a more accurate assessment of crystal growth, the combination of effects of both mass transfer and the molecular structure of the interface should be considered. These conclusions should be treated with caution not only due to the lack of sufficient experimental data but also because the data collected at the higher supersaturation studied seem to be related to a different crystal polymorphic form.

4. Conclusions

The crystal morphology and growth rates for n-docosane have been characterised for the first time. The work provides a new methodology for indexing the crystal faces of these low symmetry materials and tentative evidence is provided for solvent-induced polymorphic behaviour and kinetic roughening at higher supersaturations.

Typical growth rates were found to be in the region 0.51–9.85 μm/s over the relative supersaturation range of 0.01–0.05. The kinetic data was found to be consistent with the BCF interfacial growth mechanism.

The use of polarised optical microscopy was found to be challenging for studying this kind of materials and more suitable microscopy techniques, such as differential interference contrast (DIC), which might be expected to enhance the image contrast of such thin crystals, will be considered for future studies.

Acknowledgements

The authors gratefully acknowledge Infineum Ltd. for the funding of this research which forms part of the doctoral studies [22] of one of us (D.C.).

We also gratefully acknowledge the UK's EPSRC for the support of nucleation and crystal growth research at Leeds and Manchester through funding the Critical Mass Project: Molecules, Clusters and Crystals (Grant references EP/IO14446/1 and EP/IO13563/1).

Appendix A. Supporting information

Supplementary data associated with this article can be found in the online version at http://dx.doi.org/10.1016/j.jcrysgro.2015.01.006.

References

[1] M. Broadhurst, An analysis of the solid phase behaviour of the normal paraffins, J. Res. Nat. Bur. Stds 66A (1962) 241–249.
[2] A.R. Gerson, K.J. Roberts, J.N. Sherwood, X-ray-powder diffraction studies of alkanes – unit-cell parameters of the homologous series $C_{18}H_{38}$ to $C_{28}H_{58}$, Acta Crystallogr. B 47 (1991) 280–284.
[3] S.C. Nyburg, J.A. Potworowski, Predictions of unit cells and atomic coordinates for the n-alkanes, Acta Crystallogr. B B29 (1973) 347–352.
[4] R. Boistelle, D. Aquilano, Interaction energy and growth mechanisms on twinned and polytypic crystals of long-chain even normal-alkanes. I. interaction-energy calculations, Acta Crystallogr. A 33 (1977) 642–648.
[5] R. Boistelle, B. Simon, G. Pepe, Polytypic structures of n-$C_{28}H_{58}$ (octacosane) and n-$C_{36}H_{74}$ (hexatriacontane), Acta Crystallogr. B 32 (1976) 1240–1243.
[6] C. Rinaudo, D. Aquilano, F. Abbona, Occurrence and growth mechanism of the periodic polysynthetic twins in the even n-alkanes, J. Cryst. Growth 53 (1981) 361–368.
[7] R. Boistelle, in: E. Kaldis (Ed.), Current Topics in Material Science, North-Holland Publishing Co., Amsterdam, 1980, pp. 413–480.
[8] A.R. Gerson, K.J. Roberts, J.N. Sherwood, A.M. Taggart, G. Jackson, The role of growth environment on the crystallization of normal alkanes in the homologous series from $C_{18}H_{38}$ to $C_{29}H_{60}$, J. Cryst. Growth 128 (1993) 1176–1181.
[9] K.J. Roberts, J.N. Sherwood, A. Stewart, The nucleation of n-eicosane crystals from solutions in n-dodecane in the presence of homologous impurities, J. Cryst. Growth 102 (1990) 419–426.
[10] S.R. Craig, G.P. Hastie, K.J. Roberts, J.N. Sherwood, Investigation into the structures of some normal-alkanes within the homologous series $C_{13}H_{28}$ to $C_{60}H_{122}$ using high-resolution synchrotron x-ray-powder diffraction, J. Mater. Chem. 4 (1994) 977–981.
[11] A.R. Gerson, K.J. Roberts, J.N. Sherwood, X-ray-powder diffraction studies of normal-alkanes – a re-examination of the unit-cell parameters of $C_{24}H_{50}$ and $C_{26}H_{54}$, Acta Crystallogr. B 48 (1992) (746–746).
[12] S.R. Craig, G.P. Hastie, K.J. Roberts, A.R. Gerson, J.N. Sherwood, R.D. Tack, Investigation into the structures of binary, tertiary and quinternary-mixtures of n-alkanes and real diesel waxes using high-resolution synchrotron X-ray powder diffraction, J. Mater. Chem. 8 (1998) 859–869.
[13] S.R. Craig, G.P. Hastie, K.J. Roberts, Chain length dependent polymorphism in even number n-alkanes: line profile analysis of synchrotron powder X-ray diffraction data, J. Mater. Sci. Lett. 15 (1996) 1193–1196.
[14] S.R. Craig, G.P. Hastie, K.J. Roberts, J.N. Sherwood, R.D. Tack, R.J. Cernik, In-situ study of the solid-solid phase transitions occurring in real diesel wax crystalline systems using differential scanning calorimetry and high-resolution synchrotron X-ray powder diffraction, J. Mater. Chem. 9 (1999) 2385–2392.
[15] R. Boistelle, A. Doussoulin, Spiral growth mechanisms of (110) faces of octacosane crystals in solution, J. Cryst. Growth 33 (1976) 335–352.
[16] B. Simon, A. Grassi, R. Boistelle, Cinétique de croissance de la face (110) de la paraffine $C_{36}H_{74}$ en solution, J. Cryst. Growth 26 (1974) 77–89.
[17] H.E. Lundagermadsen, R. Boistelle, Growth-kinetics of the (001) faces of hexatriacontane ($C_{36}H_{74}$) in solution, J. Cryst. Growth 46 (1979) 681–690.
[18] M. Rubbo, R. Boistelle, Dissolution and growth-kinetics of the (001) faces of normal-hexatriacontane crystals grown from heptane, J. Cryst. Growth 51 (1981) 480–488.
[19] X.-Y. Liu, P. Bennema, On the morphology of crystals of triclinic even normal alkanes: theory and observation, J. Cryst. Growth 135 (1994) 209–223.
[20] M. Rubbo, J.N. Sherwood, An improved method for the measurement of the rates of growth and dissolution of crystals under isothermal conditions, J. Cryst. Growth 61 (1983) 210–214.
[21] T.T.H. Nguyen, R.B. Hammond, K.J. Roberts, I. Marziano, G. Nichols, Precision measurement of the growth rate and mechanism of ibuprofen {001} and {011} as a function of crystallisation environment, CrystEngComm 16 (2014) 4568–4586.
[22] D. Camacho, PhD thesis 2015, in preparation, in: Proceedings of the School of Chemical and Process Engineering, University of Leeds.
[23] W.K. Burton, N. Cabrera, F.C. Frank, The growth of crystals and the equilibrium structure of their surfaces, Philos T R Soc A (1951) 299–358.
[24] M. Ohara, R.C. Reid, Modelling Crystal Growth Rates from Solution, Prentice-Hall, Englewood Cliffs, 1973.
[25] X.Y. Liu, P. Bennema, Morphology of Crystals, Terra Scientific, Tokyo, 1987.
[26] A. Bravais, Etudes Cristallographiques, Gauthier Villars, Paris, 1866.
[27] G. Friedel, Bulletin De La Socit Franaise De Minralogie Et De Crystallographie 30 (1907).
[28] J.D.H. Donnay, D. Harker, American Mineralogist 22 (1937) 463.
[29] A.M. Taggart, F. Voogt, G. Clydesdale, K.J. Roberts, An examination of the nucleation kinetics of n-alkanes in the homologous series $C_{13}H_{28}$ to $C_{32}H_{66}$, and their relationship to structural type, associated with crystallization from stagnant melts, Langmuir 12 (1996) 5722–5728.
[30] A.R. Gerson, K.J. Roberts, J.N. Sherwood, An instrument for the examination of nucleation from solution and its application to the study of precipitation from diesel fuels and solutions of normal-alkanes, Powder Technol 65 (1991) 243–249.
[31] P. Bennema, X.Y. Liu, K. Lewtas, R.D. Tack, J.J.M. Rijpkema, K.J. Roberts, Morphology of orthorhombic long-chain normal alkanes – theory and observations, J. Cryst. Growth 121 (1992) 679–696.
[32] L.A.M.J. Jetten, H. H.J., P. Bennema, J.P. van der Eerden, On the observation of the roughening transition of organic crystals, growing from solution, J. Cryst. Growth 68 (1984) 503–516.
[33] X.Y. Liu, P. Bennema, J.P. van der Eerden, Rough-flat-rough transition of crystal surfaces, in, Nature Publishing Group, 1992, pp. 778-780.
[34] J.W. Mullin, J. Garside, Crystallization of aluminium potassium sulphate: a study in the assessment of crystallizer design data: I: single crystals growth rates,II: growth in a fluidized bed, Trans. Inst. Chem. Eng. 45 (1967) 285–295.
[35] X.Z. Wang, J.C. De Anda, K.J. Roberts, Real-time measurement of the growth rates of individual crystal facets using imaging and image analysis – a feasibility study on needle-shaped crystals of L-glutamic acid, Chem. Eng. Res. Des. 85 (2007) 921–927.
[36] A.G. Stapley, C. Himawan, W. MacNaughtan, T.G. Foster, A computational method for extracting crystallisation growth and nucleation rate data from hot stage microscope images, Cryst. Growth Des. 9 (2009) 5061–5068.
[37] C.T. Ó'Ciardhá, N.A. Mitchel, K.W. Hutton, P.J. Frawley, Determination of the crystal growth rate of paracetamol as a function of solvent composition, Ind. Eng. Chem. Res. 52 (2012) 4731–4740.
[38] S.D. Finnie, R.I. Ristic, J.N. Sherwood, A.M. Zikic, Morphological and growth rate distributions of small self-nucleated paracetamol crystals grown from pure aqueous solutions, J. Cryst. Growth 207 (1999) 308–318.
[39] D.H.M. Beiny, J.W. Mullin, K. Lewtas, Crystallisation of n-dotriacontane from hydrocarbon solution with polymeric additives, J. Cryst. Growth 102 (1990) 801–806.
[40] W. Beckmann, R. Boistelle, Growth kinetics of the (110) face of stearic acid growing from butanone solutions – pure solutions and in the presence of an emulsifier, J. Cryst. Growth 72 (1985) 621–630.
[41] W. Beckmann, Growth kinetics of the (001) and (110) faces of the b modification of stearic acid growing from n-alkanes, J. Cryst. Growth 79 (1986) 797–800.